Environ Monit Assess (2021) 193:411
https://doi.org/10.1007/s10661-021-09184-x

Responses of surface water quality to future land cover and climate changes in the Neka River basin, Northern Iran

Sharif Joorabian Shooshtari · Kamran Shayesteh · Mehdi Gholamalifard · Mahmood Azari · Juan Ignacio López-Moreno

Received: 2 December 2020 / Accepted: 1 June 2021

Abstract The spatial and temporal dimensions of environmental impacts of climate and land cover changes are two significant factors altering hydrological processes. Studying the effects of these factors on water quality, provides important insight for water resource management and optimizing land planning given increasing water scarcity and water pollution. The impact of land cover and climate changes on surface water quality was assessed for the Neka River basin in Northern Iran. The widely used Soil and Water Assessment Tool (SWAT) was applied for pollutant modeling, and was calibrated using the Sequential Uncertainty Fitting (SUFI-2) algorithm. An ensemble of 17 CMIP5 climate models under two IPCC greenhouse gas emission scenarios were selected, and future land cover change (LCC) was modeled based on the evolution that occurred in the last decades. We simulated the impacts of climate change (CC) and LCC on sediment, nitrate, and phosphate for the 2035–2065 time slice. The annual loads of sediment, phosphate, and nitrate are projected to decrease under both CC scenarios based on the inter-model average, and generally follow a pattern similar to the change in river discharge. Nitrate concentrations show an increase across all seasons, while the sediment and phosphate concentrations increase in winter and autumn under CC conditions. Results indicate that pollutants are expected to increase under LCC alone, mainly due to the expansion of the cultivated areas. Overall, it seems

S. Joorabian Shooshtari
Department of Nature Engineering, Agricultural Sciences and Natural Resources University of Khuzestan, Mollasani, Iran
e-mail: Joorabian@asnrukh.ac.ir

S. Joorabian Shooshtari · K. Shayesteh (✉)
Department of Environment, Faculty of Natural Resources and Environment, Malayer University, 65719-95863 Malayer, Hamedan, Iran
e-mail: k.shayesteh@malayeru.ac.ir; ka_shayesteh@yahoo.com

M. Gholamalifard
Department of Environment, Faculty of Natural Resources, Tarbiat Modares University, P.O. Box 46414-356, Noor, Mazandaran, Iran
e-mail: M.gholamalifard@modares.ac.ir

M. Azari
Department of Watershed Management Engineering, Faculty of Natural Resources and Environment, Ferdowsi University of Mashhad, 91779-48974 Mashhad, Iran
e-mail: Azarimahmood@yahoo.com

J. I. López-Moreno
Department of Geoenvironmental Processes and Global Change, Pyrenean Institute of Ecology, CSIC, Campus de Aula Dei, 50.059 Zaragoza, Spain
e-mail: nlopez@ipe.csic.es

Published online: 11 June 2021

CC has a greater impact than LCC on the variation of water quality variables in the Neka River basin. With a combined change in climate and land cover, the annual nitrate concentrations are expected to increase by + 19.7% and + 17.9%, under RCP 4.5 and RCP 8.5, respectively. The combined impacts of the CC and LCC caused a decline in the annual sediment and phosphate concentrations by −10.1% and −2.2% under RCP 4.5 and −9%, and −3.2% under RCP 8.5, respectively.

Keywords Catchment modeling · SWAT · Nutrients · Calibration · Neka River basin · Iran

Introduction

The hydrological impacts of climate and land cover changes on water quality are essential to understand the optimal land and water resource management (Tamm et al., 2018). Climate change is a critical issue in the current century, because it causes a significant shift in the temperature and precipitation regimes on local and global scales. Changes in these parameters have considerable impacts on the hydrology cycle (Deng et al., 2015). Warming may accelerate the evaporation rate, reducing runoff and soil moisture (Lin et al., 2007; Fan & Shibata, 2015), and it also causes shifts in the frequency and duration of hydrological droughts (Vicente-Serrano et al., 2014). Higher temperature could also accelerate the water cycle leading to changes in the precipitation patterns. Changes in the precipitation will affect the future availability of water resources, streamflow magnitude, and the quantity of nutrient transport. In addition, increased air and water temperatures induce some negative changes in the nutrient cycle, eutrophication rate, and water quality (Fan & Shibata, 2015).

The hydrological response of watersheds could be affected by land cover changes due to urbanization, influencing both water quantity and quality. One main threat to water quality and supply security is intensive agricultural development, increasing the agrochemical inputs to water bodies and creating eutrophication problems (Mehdi et al., 2015; Serpa et al., 2017). The impacts of increasing agricultural lands and urban areas are often reflected in soil integrity, nutrient fluxes, and species communities (Boix-Fayos et al., 2008; Baker & Miller, 2013), and result in reduced base flow via changing ground water portion and pathways to water bodies (Fan & Shibata, 2015). Changing land cover has apparent impacts on the hydrological cycle components (Aboelnour et al., 2020; Kibii et al., 2021), and also on soil erosion (Lenhart et al., 2003; Serpa et al., 2015; Zhang et al., 2021).

Land cover is another driving force that affects water quality (El-Khoury et al., 2015; Nguyen et al., 2019). Earlier studies revealed climate change sensitivity assessment on surface water quality (Glavan et al., 2015; Verma et al., 2015). Other studies have investigated the combined effects of future changes in land cover and climate (Mehdi et al., 2015; Molina-Navarro et al., 2014; Serpa et al., 2017). For instance, Serpa et al. (2017) analyzed the effects of climate and land cover change on water quality using SWAT in the São Lourenço watershed, Portugal. They used the outcome from ECHAM5 GCM driven by the B1 and A1B scenarios for CC simulation and applied the same storylines as CC scenarios to generate land use change scenarios. The combined land cover and CC analysis indicated declining additive effects on the pollutants, rather than change from individual pollutants alone. Mehdi et al. (2015) explored the effect of CC and LCC on nitrates and phosphorus in Bavaria, Germany, and found that the average annual NO_3^--N and TP loads increased 3- and eightfold, respectively, under combined simulations.

In Iran, a few studies have explored the standalone potential hydrological impacts of climate change (Abbaspour et al., 2009; Ashraf Vaghefi et al., 2014) and land cover alterations (Hosseini et al., 2012) on water quantity; however, only a few studies have focused on modeling the combined effects on discharge and water balance components (Joorabian Shooshtari et al., 2017; Tayebzadeh Moghadam et al., 2021). In a previous study (Joorabian Shooshtari et al., 2017), we applied the SWAT model to study how changes in the future land cover and CC have impacted the hydrological processes. The future trend of spatial distributions of various land covers was modeled using the neural network and Markov chain implemented in the Land Change Modeler (LCM), and CMIP5 models were used to explore the effects of climate change on precipitation and temperature under RCP 4.5 and RCP 8.5 scenarios. Till now, no research has addressed the combined impacts of these drivers on the quality of water modeling in Iran. Pirnia et al. (2019) studied the impacts of climatic change and human activities

on stream flow in the Haraz River basin, Iran and found that these variables contributed to 34.78% and 65.21%, respectively, of changes in annual stream flow based on the SWAT model simulations. Choubin et al. (2019) showed that the stream flow regionalization by the SWAT model has acceptable performance in ungauged basins of Iran's Karkheh River watershed. Tayebzadeh Moghadam et al. (2021) used the SWAT model to simulate the impacts of climate and land use changes on the water balance components for the Taleghan Catchment in Iran. They reported that the CC has more severe impact on water yield than LCC, whereas LCC has a more essential effect on sediment yield. In the present study, we address the questions of the response of the surface water quality under various climate emission scenarios and future land cover with the aim of evaluating the relative strength of their impacts and integrated approach of hydrological modeling using SWAT to quantify the contribution of combined effects in the Neka River watershed in the north of Iran. In the current research, we used the previously satisfactory calibrated SWAT model for the river discharge in this area (Joorabian Shooshtari et al., 2017) to calibrate and validate the sediment and nutrient loads, including nitrate and phosphate. The simulation results of the LCC based on LCM and projected changes in the temperature and precipitation by the various CMIP5 models obtained from previous research were used to assess the effects of LCC and CC on the water quality parameters in the Neka River basin.

The objective of this study includes the development of a land cover scenario for the year 2050 using LCM based on Markov chain matrix and MLP neural network for generating the likelihood of transitioning and projected climatic changes for the same time horizon through using the Coupled Model Intercomparison Project Phase 5 (CMIP5) models and Representative Concentration Pathway (RCP) scenarios from the Intergovernmental Panel on Climate Change Fifth Assessment Report (AR5).

Materials and methods

Study area

The study basin covers 1871 km^2 encompassed within 53° 17′ 30″–54° 44′ 22″E and 36° 27′ 46″–36° 41′ 8″N. It is part of northern Iran's Hyrcanian Forest, in the Neka River basin, Mazandaran and Golestan Provinces (Fig. 1) (Joorabian Shooshtari et al., 2012). The area, located between the Caspian Sea on the north and the Alborz Mountains to the south, is the major source of irrigation water for the extensively cultivated area of Neka County, and it discharges into the Caspian Sea. The

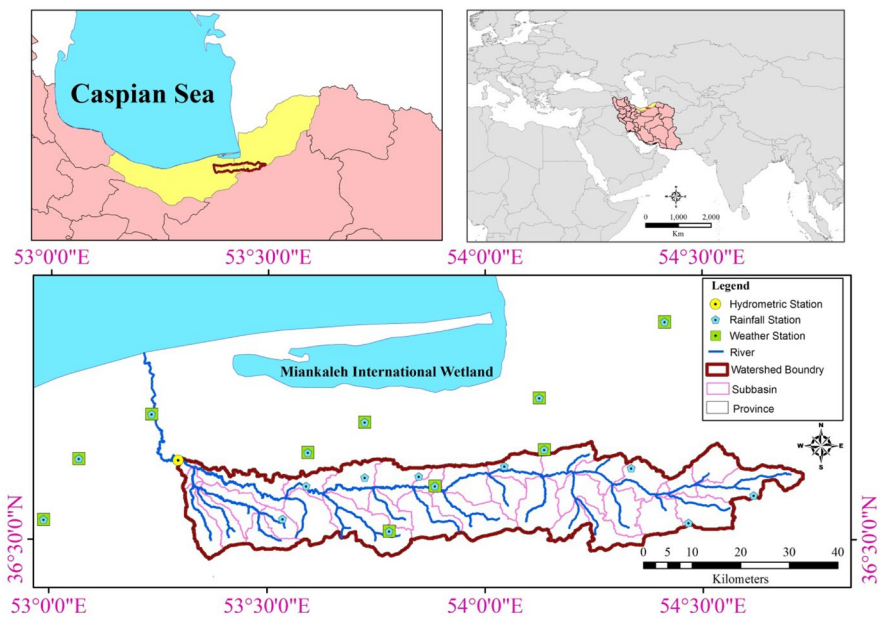

Fig. 1 Location of the study area in Iran

mean annual temperature is 17 °C, with the minimum and maximum temperatures in January and August, respectively. The annual precipitation of the watershed is 600 mm (Ghanbarpour et al., 2014). The annual rainfall cycle is at the maximum in autumn and minimum in summer with a decreasing trend in high elevation. The land cover is primarily rangelands (44%), followed by Hyrcanian forest (36%), and cultivated land (18%) (Joorabian Shooshtari et al., 2018). The use of fertilizer for agriculture is one of the main nonpoint sources of water quality reduction in this watershed. For instance, the mean annual use of fertilizers for Mazandaran Province exceeds 170 tons (Rajaei et al., 2017). The Neka River is the most important source of water for domestic, industrial, and agricultural use in the region. Neka County is ranked second in wheat production in Mazandaran Province which is associated with heavy use of nitrogen and phosphate fertilizers in agricultural areas. Therefore, this basin, near the Caspian Sea, was chosen for this research to obtain deeper insight for determining the amount of nutrients exported from this catchment under future conditions.

Climate change

In the current study, monthly temperature and precipitation were extracted for the 1980–2010 period as a control, and from 2035–2065 as the future time horizon, from a total of 17-member ensembles of CMIP5 models. These models include BNU-ESM, CanESM2, CCSM4, CESM1-CAM5, CNRM-CM5, CSIRO-Mk3-6–0, EC-EARTH, FGOALS-g2, GFDL-ESM2G, GISS-E2-H, GISS-E2-R, HadGEM2-AO, IPSL-CM5A-LR, MIROC5, MPIESM-LR, MRI-CGCM3, and NorESM1-M. We used new moderate (RCP 4.5) and intensive (RCP 8.5) emission scenarios published by the AR5 IPCC (2013). RCP 4.5 and RCP 8.5 are characterized by radiative force of 4.5 and 8.5 W/m^2, respectively; CO_2-equivalent concentrations are 650 and 1370 ppmv, respectively, by the year 2100. To obtain the inter-model seasonal variability in temperature and precipitation of several climate models, multi-model delta averages in the 10th and 90th percentiles were calculated. Delta change approach is a relatively simple method for constructing regional CC scenarios, which have been implemented for rapid assessment of CC effects (Wilby & Harris, 2006).

The differences between the observed (1980–2010) and GCM outputs (2035–2065) were applied to daily observed historical time series data (2003–2014) obtained from meteorological stations of this watershed (Fowler et al., 2007). Then, the new run in SWAT simulations was applied using the modified climate series for each GCM, to investigate the impacts of CC on the water quality parameters. This stage was applied to reduce the uncertainty in the calculations. Therefore, the SWAT model was run for each GCM model, and then the average, 10th, and 90th percentiles for output values of all SWAT runs; values such as sediment and water quality were calculated. The SWAT model was run 34 times (17 CMIP5 models and two RCPs) for each water quality parameters under climate change alone (102 times for three parameters (sediment, nitrate, and phosphate) in total), and it, the same number of runs, was used under a combined change of climate and land cover.

We computed the R10mm index (yearly count of days with precipitation of at least 10 mm) for the selected climate models of 2035–2065 relative to the reference period (1980–2010) in order to investigate future precipitation frequency changes. Changes in precipitation extremes can lead to significant impacts on sediment yields and nutrient exports.

Land cover change

LCM was applied to identify the trends in future LCCs in the Neka River basin. LCM models future land cover using the historical trend of change and transition potential map for each land cover class (Anand et al., 2018). The land cover maps for the years 1984 and 2001 were used to develop the land cover for 2010. The model's performance was evaluated comparing the observed and predicted land cover in 2010 (presented in Joorabian Shooshtari et al., 2017). After achieving reasonable accuracy, the projected land cover for 2050 was modeled using data from 2001 to 2010, based on multi-objective land allocation. Topographic variables (slope, elevation), proximity factors (distance to residential areas, forest, agricultural land, rangelands, major roads, fluvial streams), and the empirical likelihood of change between 1984 and 2001 were considered influential variables determining land cover changes. Cramer's V coefficient was executed to test the strength of the association between variables and land cover categories (Joorabian Shooshtari & Gholamalifard,

2015). We observed slope factor with lowest (Cramer's = 0.0971) and empirical likelihood to change with highest (Cramer's = 0.5742) overall V predictive power (Joorabian Shooshtari et al., 2018). A total of six sub-models were used to produce transition potential using extensively enhanced multi-layer perceptron (MLP). In subsequent research (Joorabian Shooshtari et al., 2018), a similarity-weighted instance-based machine learning algorithm in LCM was successfully applied to predict multiple transitions among land cover classes. In the current work, MLP neural network in LCM, known to be more robust than other algorithms, was used to generate a transition potential surface for each land cover transition (Eastman et al., 2005; Sangermano et al., 2012). Validation of the MLP after 10,000 iterations showed the accuracy rate to be above 88% in all sub-models, and the lowest and highest values were 88.10 and 95.78%, respectively. Then, the 2050 land cover was predicted by applying results obtained from transition susceptibility maps and calculation of transition matrix using Markov chain (Mas et al., 2014). Land cover change analysis between 2010 and 2050 illustrates the reduction of the forest area by 12.1%, while the increase in an agricultural area (12.2% of the agricultural area), residential (41% of the residential area), and rangelands (4.8% of the rangeland area) could be expected (Fig. 2). Figure 3 shows the results of changes for each land cover class among three study periods.

SWAT hydrologic model

The ArcGIS interface for SWAT, ArcSWAT, v. 2012 was applied to simulate hydrology and surface water quality (sediment, nitrate, and phosphate) in the Neka River basin. The eco-hydrological model SWAT is a high-performance tool for achieving in-depth insight into water quality dynamics under future environmental conditions from catchments of various sizes. In the SWAT, the catchment is divided into multiple sub-basins, and subsequently into smaller units called hydrologic response units (HRUs) as the basic calculation elements that possess homogeneous soil type, land use, and slope characteristics (Fan & Shibata, 2015; Neitsch et al., 2011). The water balance is calculated at an HRU and stored in four storage volumes. In the current study, surface runoff in each HRU is estimated with a modified Soil Conservation Service Curve Number method using daily rainfall data. Potential evapotranspiration is computed using the Hargreaves method (a temperature-based model) due to the readily available data.

The sediment yield and soil erosion for each HRU in SWAT are based on the modified soil loss equation (Williams and Berndt, 1977) (Eq. (1)):

$$sed = 11.8\left(Q_{surf}.q_{peak}.area_{HRU}\right)^{0.56}.K_{USLE}.C_{USLE}.P_{USLE}.LS_{USLE}.CFRG \quad (1)$$

In Eq. (1) *sed* is the sediment yield for a day (metric tons), Q_{surf} is the volume of surface runoff (mm ha^{-1}), q_{peak} is the peak runoff rate ($m^3\ s^{-1}$), $area_{HRU}$ is the area of HRU (ha), K_{USLE} is the USLE soil erodibility factor, C_{USLE} is the USLE cover and management factor, P_{USLE} is the USLE support practice factor, L_{USLE} is the USLE topographic factor, and CFRG is the coarse fragment factor (Neitsch et al., 2011).

The nutrient cycle sub-model is similar to those of the Environmental Policy Integrated Climate (EPIC) model (Abbaspour et al., 2007).

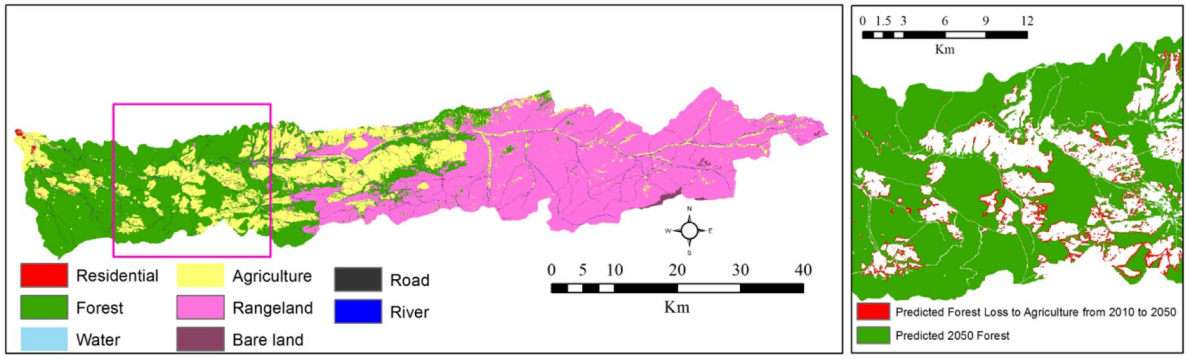

Fig. 2 Scenery of land cover simulated by 2050 and forest conversion to agriculture between 2010 and 2050

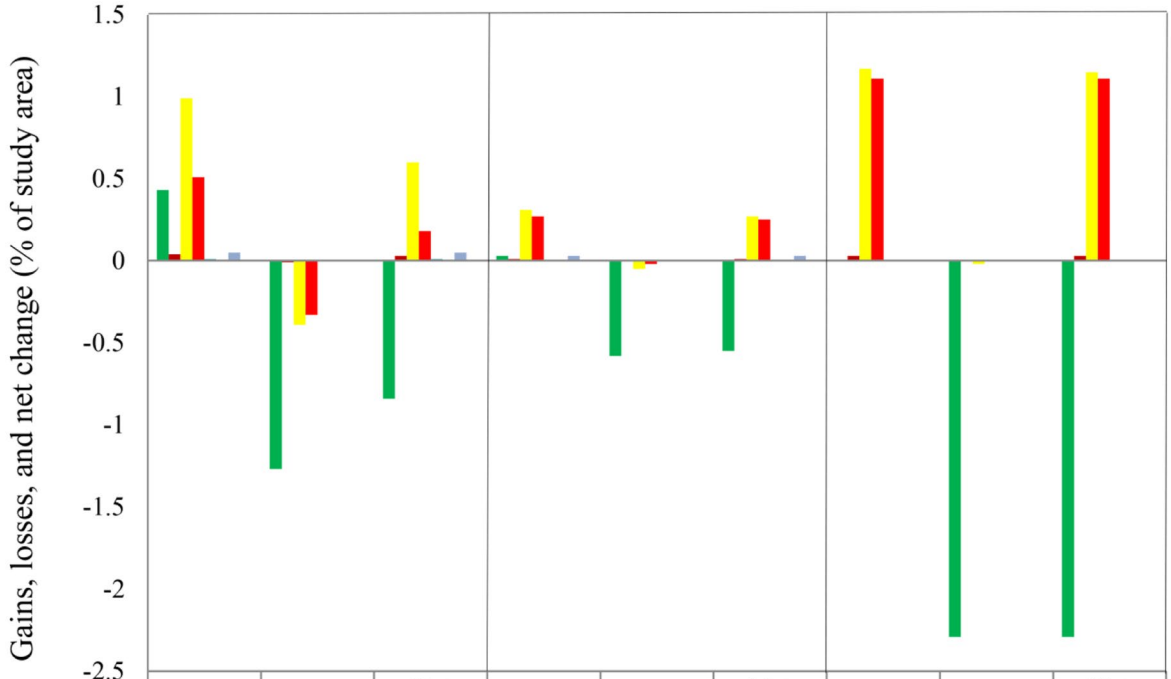

	Gains	Losses	Net change	Gains	Losses	Net change	Gains	Losses	Net change
	1984-2001			2001-2010			2010-2050		
Forest	0.43	-1.27	-0.84	0.03	-0.58	-0.55	0	-2.29	-2.29
Residential	0.04	-0.01	0.03	0.01	0	0.01	0.03	0	0.03
Agriculture	0.99	-0.39	0.6	0.31	-0.05	0.27	1.17	-0.02	1.15
Rangeland	0.51	-0.33	0.18	0.27	-0.02	0.25	1.11	0	1.11
Bare land	0.01	0	0.01	0	0	0	0	0	0
Water	0	0	0	0	0	0	0	0	0
Road	0.05	0	0.05	0.03	0	0.03	0	0	0
River	0	0	0	0	0	0	0	0	0

Fig. 3 Net change, gains, and losses 1984–2001, 2001–2010, and 2010–2050 (percentage of the study area)

SWAT inputs were the elevation data (DEM) from the Aster Global DEM (30-m resolution), and soil data from the world SOIL of FAO (Food and Agriculture Organization) database (10-km resolution). Daily temperature and rainfall data are available from 2003 to 2014 at 10 and 19 stations, respectively, in the study area. A threshold value of 10% for soil and slope and 0% for land cover were selected to produce the HRUs. Five classes of slope (0–5, 5–12, 12–30, 30–60, and > 60) were utilized in the HRU definition. Thirty-five sub-watersheds were delineated using a threshold value of 3000 ha.

Table 1 provides agriculture operations adapted for simulation of winter wheat and winter barley. The management operation scheme applied in SWAT is based on the average long-term data from the Ministry of Agriculture of Mazandaran and Golestan Provinces. The amount of fertilizer application with urea and with 18–46-00 fertilizer was 90 kg ha^{-1} and 50 kg ha^{-1}, respectively, in the study watershed.

In the current study, the Sequential Uncertainty Fitting algorithm in SWAT-CUP software was used for calibration, validation, and uncertainty assessment. It is able to analyze the parallel processing of

Table 1 Properties of management operations for winter wheat and winter barley in the Neka River basin

Crop type	Year	Operation type	Date	Operation attributes
Winter wheat	1	Tillage	27 September	Mouldboard plough
	1	Planting	11 November	-
	1	Fertilizer	11 November	Urea, 30 kg/ha
	1	Fertilizer	11 November	18–46-00, 50 kg/ha
	1	Fertilizer	26 December	Urea, 30 kg/ha
	1	Fertilizer	25 April	Urea, 30 kg/ha
	1	Harvest	17 June	-
Winter barley	1	Tillage	12 September	Mouldboard plough
	1	Planting	9 October	-
	1	Fertilizer	9 October	Urea, 30 kg/ha
	1	Fertilizer	9 October	18–46-00, 50 kg/ha
	1	Fertilizer	23 November	Urea, 30 kg/ha
	1	Fertilizer	22 March	Urea, 30 kg/ha
	1	Harvest	10 May	-

multi-site calibration and ascertains uncertainties through the sequential and fitting processes (Wu & Chen, 2015). To compare monthly measured and simulated data, the Nash–Sutcliffe efficiency parameter (ENS), PBIAS, and the coefficient of determination (R^2) were used (Ficklin et al., 2013) (Eqs. (2)–(3)).

$$ENS = 1 - \sum_{i=1}^{n}\left(O_i - P_i\right)^2 / \sum_{i=1}^{n}\left(\mathrm{O}_i - \overline{O}_i\right)\Big)^2 \quad (2)$$

$$PBIAS = \left(\sum_{i=1}^{n}\left(O_i - P_i\right) / \sum_{i=1}^{n} O_i\right) \times 100 \quad (3)$$

$$R^2 = \left\{ \sum_{i=1}^{n}\left(O_i - \overline{O}_i\right)\left(P_i - \overline{P}_i\right) / \left[\sum_{i=1}^{n}\left(O_i - \overline{O}_i\right)^2\right]^{0.5}\left[\sum_{i-1}^{n}\left(P_i - \overline{P}_i\right)^2\right]^{0.5} \right\}^2 \quad (4)$$

where O_i and P_i are the observed and predicted values, $\overline{O}_i$ is the mean value of the observed data, and n is the number of data. Two uncertainty indices are used to evaluate the goodness of model performance in terms of calibration and uncertainty level: the *p*-factor and the *r*-factor. We used the calibrated and validated SWAT model for discharge, as developed by Joorabian Shooshtari et al. (2017) in the current research, and the detailed SWAT model setup and validation procedure can be obtained there. The observed sediment data from 2003 to 2010 were used as calibration for the outlet catchment, while a 4-year sediment dataset (2011–2014) was used for validation, and the first 3 years were also dedicated as a warm-up.

The measured nutrient data were available only once or twice per month in the Neka River basin, while the daily time series water quality data were used to calculate monthly average needs for SWAT nutrient calibration. Therefore, the regression model Load Estimator (LOADEST), a FORTRAN-based load estimation software (Runkel et al., 2004) developed by USGS, was used in order to generate a complete monthly time series of nitrate and phosphate from instantaneous discharge and nutrient data (Niraula et al., 2013). SWAT parameters were calibrated using NO_3^- and PO_4^{3-} data for the period 2013–2014 and validated using data from 2012.

Results

Model performance

The comparison of simulated and observed river discharge on monthly data values during the calibration and validation periods revealed satisfactorily simulated by the evaluation statistics of ENS and R^2

Table 2 List of SWAT's parameters and their best values used for SUFI-2

Variable	Parameter name	Definition	Best value
Sediment	v__FILTERW.mgt	Width of edge of field filter strip	26.418
	v__HRU_SLP.hru	Average slope steepness	0.070
	v__SLSUBBSN.hru	Average slope length	10
	v__LAT_SED.hru	Sediment concentration in lateral flow and groundwater flow	1995.26
	r__USLE_K().sol	USLE equation soil erodibility (K) factor	0.159
	v__SPEXP.bsn	Channel re-entrained exponent parameter	1.314
	v__SPCON.bsn	Channel re-entrained linear parameter	0.006
Nitrate	v__CMN.bsn	Rate factor for humus mineralization of active organic nitrogen	0.0023
	v__ANION_EXCL.sol	Fraction of porosity from which anions are excluded	0.9005
	v__RCN.bsn	Concentration of nitrogen in rainfall	1.075
Phosphate	v__RS5.swq	Organic phosphorus settling rate in the reach at 20 °C	0.089
	v__RS2.swq	Benthic (sediment) source rate for dissolved phosphorus in the reach at 20 °C	0.091
	v__LAT_ORGP.gw	Organic P in baseflow	0.795
	v__GWSOLP.gw	Concentration of soluble phosphorus in groundwater contribution to streamflow from subbasin	0.00083
	v__BC4.swq	Rate constant for mineralization of organic P to dissolved P in the reach at 20 °C	0.1405

(Joorabian Shooshtari et al., 2017). Table 2 shows the fitted values of the most sensitive parameters used for simulating water quality in the Neka River basin. Results for performance metrics of surface water quality modeling for the simulation period are shown in Table 3. Comparing monthly observed and simulated values of water quality showed that the trend of their values matched well (Fig. 4). Similar to the discharge, the sediment simulation using SWAT is also acceptable in terms of the 96% and 80% of data being bracketed by 95PPU for calibration and validation periods, respectively (Fig. 4). Sediment simulation performance for the calibration period was better than that of the validation period, in terms of NSE, R^2, and PBIAS (Fig. 4). The dynamics of sediments and nutrients were adequately represented by the model, although the simulated phosphate was overall higher during the calibration and validation periods (Fig. 4). Statistically (according to values of NSE and R^2), the model showed better performance for the sediment rather than for nutrients. Nitrate calibration with r-factor less than 1 generally shows good calibration results (Table 3), while 29% of the measured data were bracketed by the 95PPU, which indicates that the actual uncertainty is larger than that shown (Fig. 4).

ENS for sediment was 0.83 and 0.73 for the calibration and validation periods, respectively, presenting the acceptable model performance. Furthermore, R^2 coefficient values were 0.83 and 0.74 for both periods, indicating a relatively high correlation between the monthly observed and predicted sediment data. The ENS performance rating for the monthly calibration of nitrate and phosphate was 0.69 and 0.56 for the calibration period, and 0.52 and 0.63 for the validation period. The R^2 values for nitrate and phosphate were 0.74 and 0.57 for the calibration period and 0.56 and 0.66 for the validation period. R^2 values for all nutrient loads' calibration and validation runs were higher than 0.5 (Table 3).

Table 3 Goodness-of-fit indicator scores for monthly water quality simulation results

Variable	Calibration					Validation				
	NSE	R^2	*p*-factor	*r*-factor	PBIAS	NSE	R^2	*p*-factor	*r*-factor	PBIAS
Sediment	0.83	0.83	0.96	1.20	+4.7	0.73	0.74	0.80	1.20	−8.0
Nitrate	0.69	0.74	0.29	0.45	−16.9	0.52	0.56	0.83	0.44	15.1
Phosphate	0.56	0.57	0.62	0.81	−5.9	0.63	0.66	0.92	2.61	−12.7

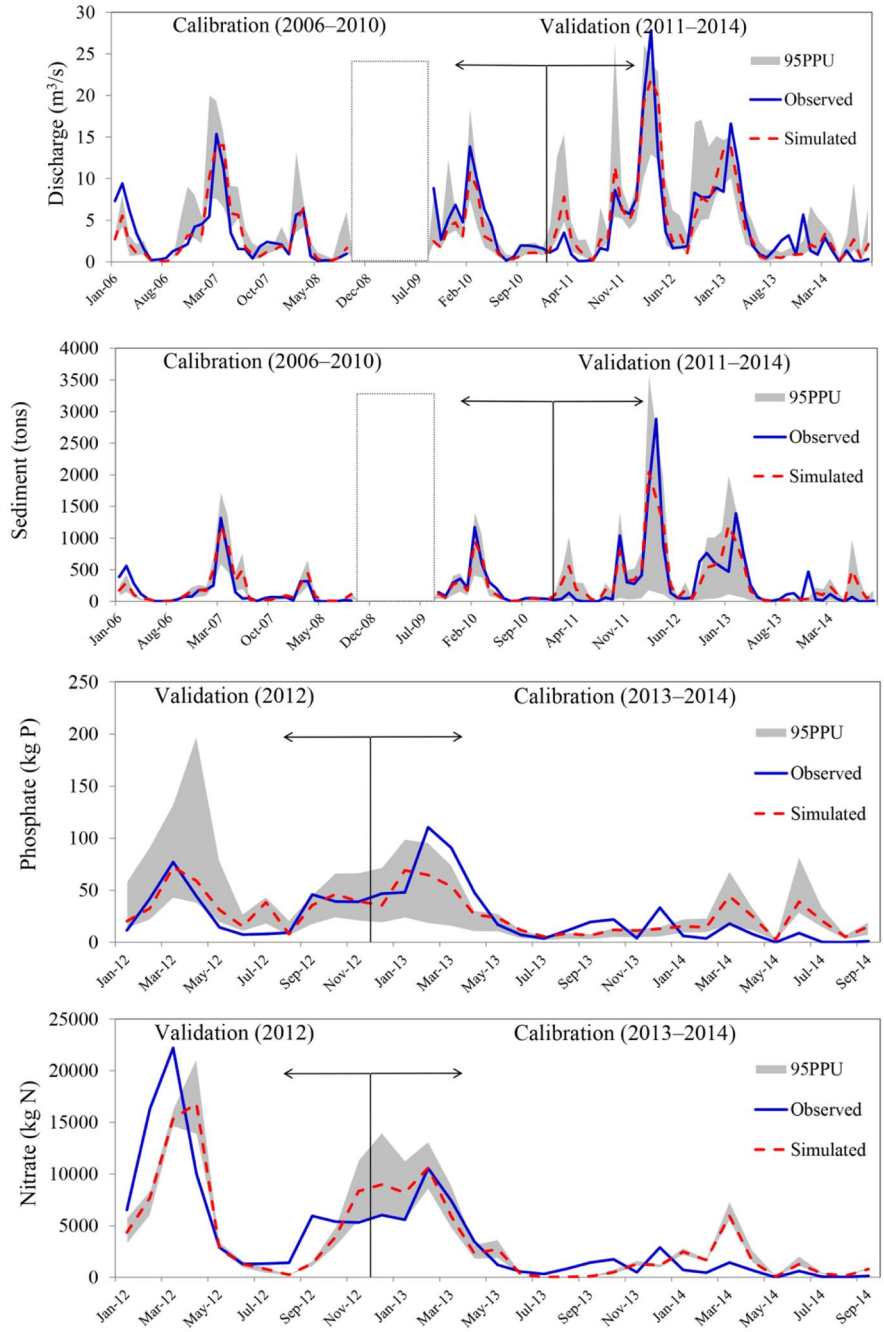

Fig. 4 Comparison of monthly averaged simulated and observed values of sediment, phosphate, and nitrate of Neka River basin for calibration, validation, and 95% prediction uncertainty (95PPU)

For river discharge, a *p*-factor higher than 70% or 75% and an *r*-factor of around 1 have been recommended. For the sediment parameter, the lower *p*-factor and higher *r*-factor values could also be adequate (Abbaspour, 2015). The *p*-factor of nitrate for the validation period was higher than that of the calibration period, representing that the actual uncertainty was higher in the calibration (Fig. 4). The model indicated great uncertainty for phosphate for the validation period given its high *r*-factor (2.61). The 62% and 92% of the observed data were bracketed by the 95PPU for the phosphate simulation results during the calibration and validation periods, respectively (Fig. 4).

PBIAS suggests that the model tends to underestimate sediment load for the calibration and overestimate for the validation period (Table 3). The observed and simulated nitrate values showed over/underestimation for the calibration/validation, while phosphate simulation revealed overestimation for both periods (Fig. 4). A noticeable uncertainty is associated with simultaneous calibration for various variables.

Climate change

Figure 5 shows the seasonal temperature and precipitation changes from various climate models for the period 2035–2065 relative to the reference period (1980–2010) under RCP 4.5 and RCP 8.5 scenarios in the Neka River basin. The projections revealed a mean 1.7 °C and 2.3 °C increase in the annual temperature under RCP 4.5 and RCP 8.5, respectively. Future CC simulations showed that the highest and lowest warming in temperature would occur in summer (June, July, August) and winter (December, January, February), respectively, under both scenarios. Simulations' results indicated mean annual precipitation change of + 0.7% but with a large inter-model variability (ranges from − 13.3% to + 19%) and + 3.4% (ranges from − 11.2% to + 17.4%) for RCP 4.5 and RCP 8.5, together with greatest decrease and increase in summer (RCP 4.5 scenario: − 13%; RCP 8.5 scenario: − 21%) and winter (RCP 4.5 scenario: 4%; RCP 8.5 scenario: 9%), respectively. It can be seen that precipitation indicated a high degree of uncertainty among various climate models. The multi-model precipitation simulations suggest a change in summer, in the range of − 168% to + 38% for RCP 4.5 and − 123%

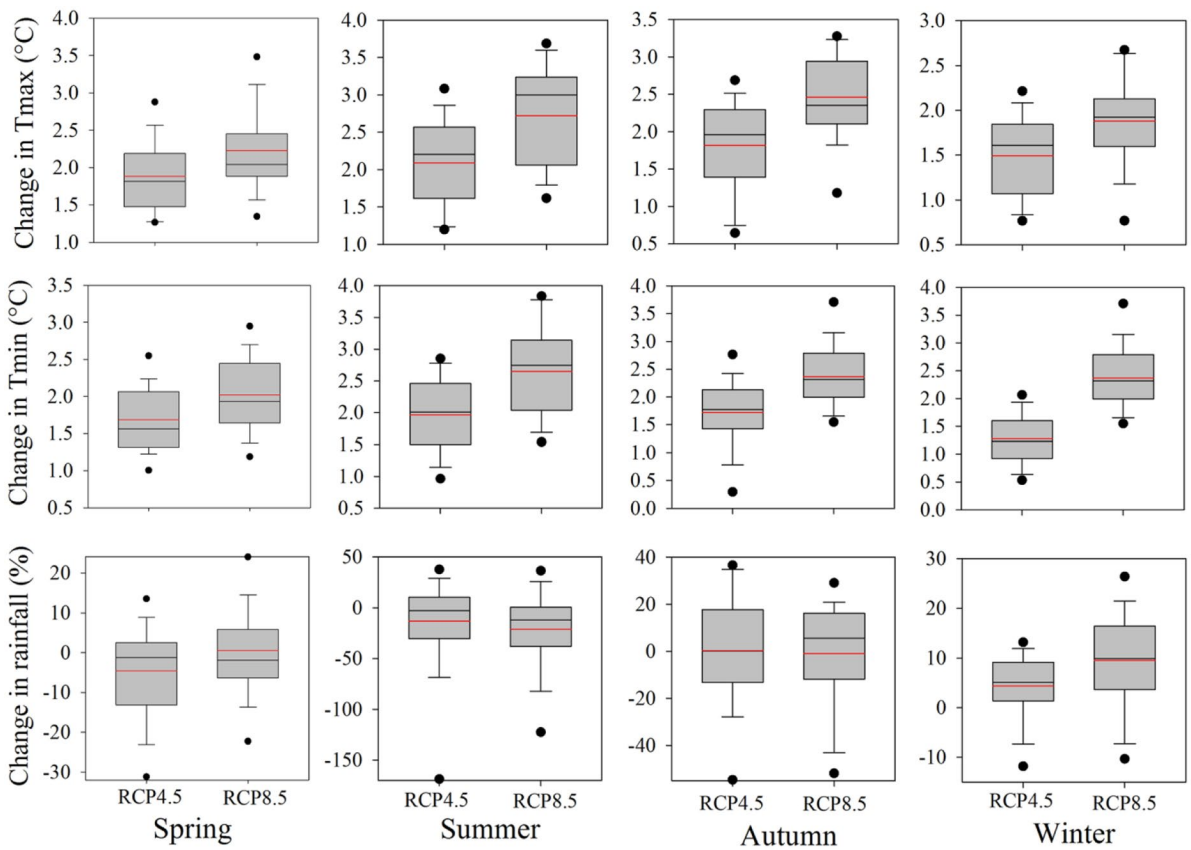

Fig. 5 Box plot showing seasonal changes among the various climate models in temperature and precipitation under RCP 4.5 and RCP 8.5 (red line indicates average). The range indicated by the box plots shows the 75th and 25th percentiles, and the dots denote the extremes

Table 4 Percent change for R10mm index in RCP 4.5 and RCP 8.5 scenarios for selected climate models in the Neka River basin

Model	RCP 4.5	RCP 8.5
CNRM-C5	20.6	2.3
CSIRO-Mk3-6–0	20	112.9
MIROC5	4.1	6.2
MRI-CGCM3	22.4	27.6
NorESM1-M	0	−8.8
Can-ESM2	67.3	41.3
CCSM4	10.2	14.9

to + 36% for RCP 8.5 (Fig. 5). The variability of precipitation simulations from the 17 CMIP5 models was larger than those of the temperature projections, especially in summer (Fig. 5).

The R10mm index shows different results among various selected climate models for the period 2035–2065 relative to the 1980–2010 period (Table 4). For instance, the CSIRO-Mk3-6–0 and NorESM1-M models represented + 112% and −9% changes, respectively, for the RCP 8.5 scenario. These results indicate a high degree of uncertainty among various models in simulation of trends of precipitation extremes in the study region.

Impacts of CC and LCC on sediment yield

The mean simulated annual sediment yield in the main outlet was 207.1 tons during 2006−2014 (Table 5). The projected annual sediment yield showed a decline under both the RCP 4.5 (8.1%) and RCP 8.5 (1.6%) scenarios, and the same land cover based on the inter-model average. CC scenarios showed their highest decrease in June for RCP 4.5 (39%, from 90.4 to 55.1 tons) and RCP 8.5 (57.6%, from 90.4 to 38.3 tons) scenarios, and the highest increase in December for RCP 4.5 (12%, from 198 to 221.8 tons) and January for RCP 8.5 (25.4%, from 255.2 to 320.1 tons) (Fig. 6). The inter-model average for CC alone showed a significant reduction in the sediment yield concerning the baseline conditions [observed (2003–2014)] climate data, with land cover for 2010, which ranged from 11.8% [autumn (September, October, November)] to 31.9% (summer) for RCP 4.5 and 6.5% [spring (March, April, May)] to 43% (summer) for RCP 8.5, which is observed for all seasons except winter. Sediment yield is projected to increase in winter under two RCPs (RCP 4.5 scenario: 1.4%; RCP 8.5 scenario: 15.4%) based on the inter-model average. For the sediment yield, annual decreases of 48%, and 44.4%, and an annual increase of 30.7%, and 47.7%, respectively, are projected for the 10th and 90th percentiles of the multi-model under RCP 4.5 and RCP 8.5 with 2010 land cover. These values marked variability among the various CMIP5 models in the forecasting of sediment loads. The model results showed that the ranges of change in mean annual sediment yield were 115.2 and 305.9 tons in the 10th and 90th percentiles of the climate models under RCP 8.5 (207.1 tons in the baseline).

When CC was combined with LCC, mean annual sediment yields showed a −6.3% and + 1.6% change under both scenarios, based on the inter-model average with change of −46.3% (10^{th} percentiles) and + 34.2% (90^{th} percentiles) for RCP 4.5 and −41.9% (10^{th} percentiles) and + 52.1% (90^{th} percentiles) for RCP 8.5. Results of simulating sediment load under RCP 4.5 with 2050 land cover demonstrated the greatest reduction, 45.7% (from 90.4 to 49.1 tons) in June, and the greatest increase, 17.1% (from 198 to 231.9 tons) in December (Fig. 7). Results indicated an annual sediment load of 111.1 tons for the 10th percentile and 278 tons for the 90th percentile under RCP 4.5 and future land cover.

Table 5 Results of annual mean water quantity and quality parameters under LCC alone, CC alone, and combined impacts of CC and LCC based on the inter-model average

Scenario	Simulation	Streamflow (m^3/s)	Sediment (tons)	Nitrate (kg N)	Phosphate (kg P)
Reference	Baseline	3.30	207.09	727.78	28.09
2050 LCC	LCC	3.41	215.14	751.13	28.70
RCP 4.5	CC	3.02	190.23	713.89	25.51
	CC + LCC	3.07	193.99	732.00	25.62
RCP 8.5	CC	3.19	203.78	725.61	26.34
	CC + LCC	3.29	210.55	750.02	26.87

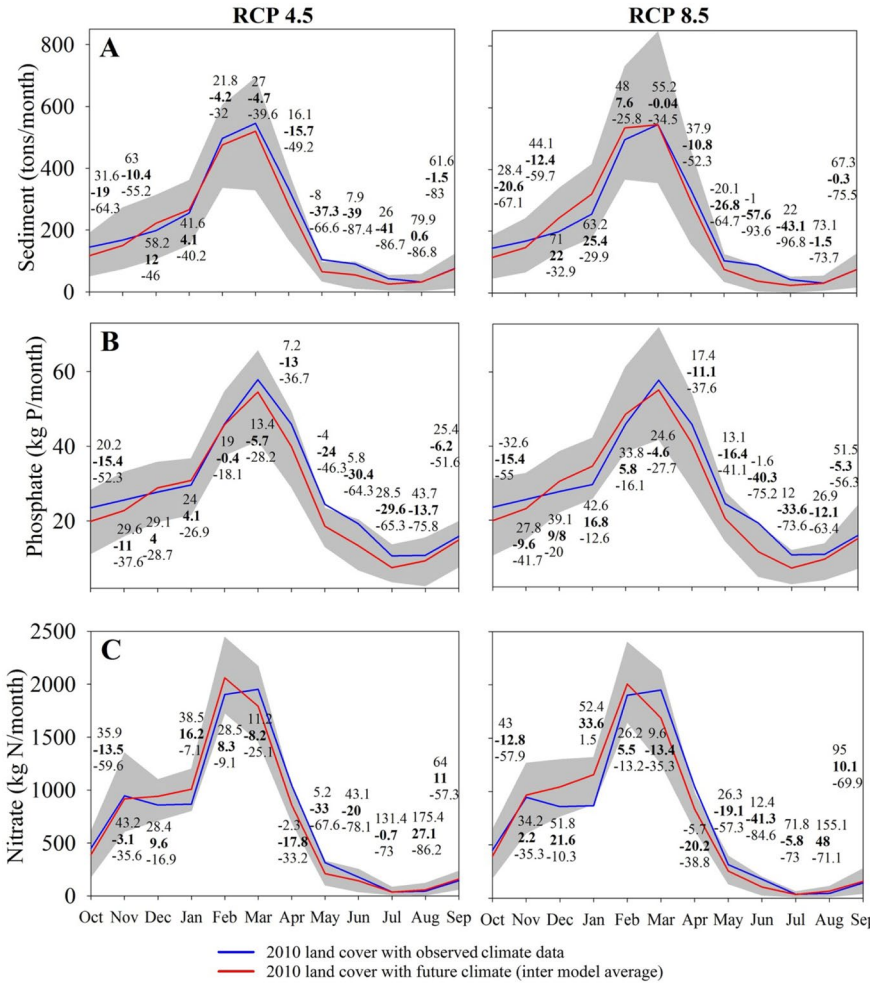

Fig. 6 SWAT simulation for **A** sediment load, **B** phosphate load, and **C** nitrate load under RCP 4.5 and RCP 8.5 scenarios and 2010 land cover. The grey band represents the 90th and 10th percentiles for various CMIP5 models. The numbers show the average change (in percent) among the various models (in bold), and the 90th (upper) and 10th (lower) percentiles

The average annual sediment concentration was 25.1 mg l^{-1} under baseline climate conditions with 2010 land cover. (SWAT output gives sediment yields in tons and flow in m^3/s. With these two, the concentration in mg l^{-1} can be calculated). The simulated results of future sediment concentrations show a decrease in the annual change by 8.6% (22.9 mg l^{-1}) and 8.5% (23.0 mg l^{-1}) under both scenarios, respectively. RCP 4.5 and RCP 8.5 showed an increase in the sediment concentration for winter and autumn and a decrease for spring and summer. The predicted sediment concentrations for spring and summer under RCP 4.5 (RCP 8.5) scenario alone were 21.8 mg l^{-1} (21.6 mg l^{-1}) and 17.3 mg l^{-1} (16.1 mg l^{-1}), respectively, while the average concentrations of sediment were 22.8 mg l^{-1} in spring and 26.1 mg l^{-1} in summer under the baseline conditions. When the LCC scenario was combined with RCP 4.5, simulated sediment concentration for the summer season displayed a significant reduction from 26.1 mg l^{-1} to 16.5 mg l^{-1}, whereas in combination with the RCP 8.5 simulations showed a reduction by −38.8% (from 26.1 mg l^{-1} to 15.9 mg l^{-1}).

The simulated mean sediment concentrations were significantly lower in June compared with the baseline conditions for CC alone and CC combined with LCC scenarios. Relative to baseline conditions, when including the climate change simulations for the RCP 8.5 scenario combined with land cover for 2050, the results revealed a −64.5% reduction of the concentration of sediment in June (from 45 mg l^{-1} in baseline to 16 mg l^{-1} in the predicted scenario) (Fig. 8). The highest increase in the exhibited sediment concentrations occurred

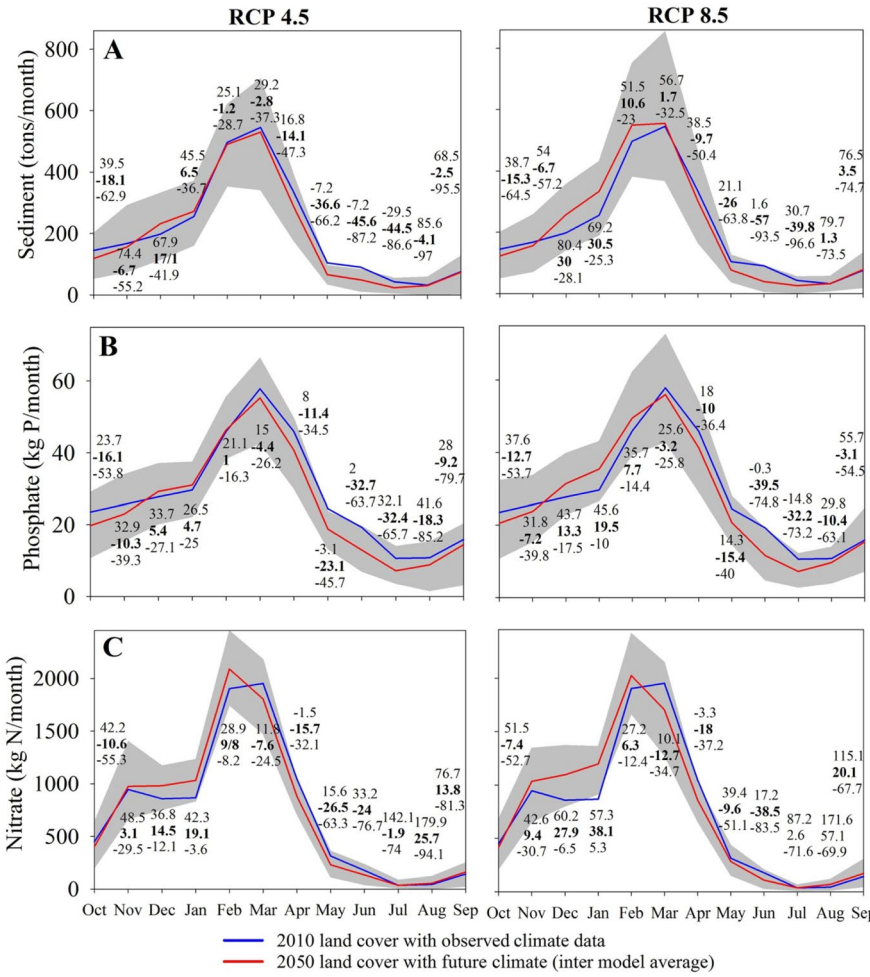

Fig. 7 SWAT simulation for **A** sediment load, **B** phosphate load, and **C** nitrate load under the combined effect of land cover change and the RCP 4.5 and RCP 8.5 scenarios. The grey band represents the 90th and 10th percentiles for various CMIP5 models. See Fig. 6 for details

in August under RCP 4.5 alone (from 18.1 mg l^{-1} in baseline to 20 mg l^{-1}), RCP 8.5 alone (from 18.1 to 21.5 mg l^{-1}), and the combination of RCP 8.5 climate scenario and future land cover (up to 21.2 mg l^{-1}) with respect to the current condition based on the average of various CMIP5 model deltas, whereas December showed the highest increase in RCP 4.5 simulations combined with land cover for 2050 (from 24.1 to 26.3 mg l^{-1}) (Fig. 8).

The average annual predicted sediment yield increased by 3.9% under simulated land cover for the year 2050 as compared with land cover for the year 2010; with climatic variables kept constant, monthly sediment yield is simulated to range from + 0.34% to + 9.3%. The sediment concentration was 21.9 mg l^{-1} in May for the 2010 land cover but decreased to 21.0 mg l^{-1} for the 2050 land cover with observed climate data (the highest decrease is projected to occur in May). The concentration of sediment showed its largest increase in December from 24.1 mg l^{-1} in baseline to 24.3 mg l^{-1} in 2050 land cover.

Impacts of isolated CC and LCC on nutrient loads

The annual loads of NO_3^- and PO_4^{3-} were 728 kg N and 28 kg P in the outlet of the basin for the period 2006–2014 (Table 5). Monthly change in nutrient loads is presented graphically in Fig. 6. RCP 4.5 and RCP 8.5 indicated a 1.9% (from 727.8 to 713.89 kg N) and a 0.3% (from 727.8 to 725.6 kg N) reduction of the annual NO_3^- load. The seasonal projections suggest increases in NO_3^- and PO_4^{3-} loads during winter under both scenarios; the rest of the seasons showed a decrease in these loads based on the inter-model average. Under both

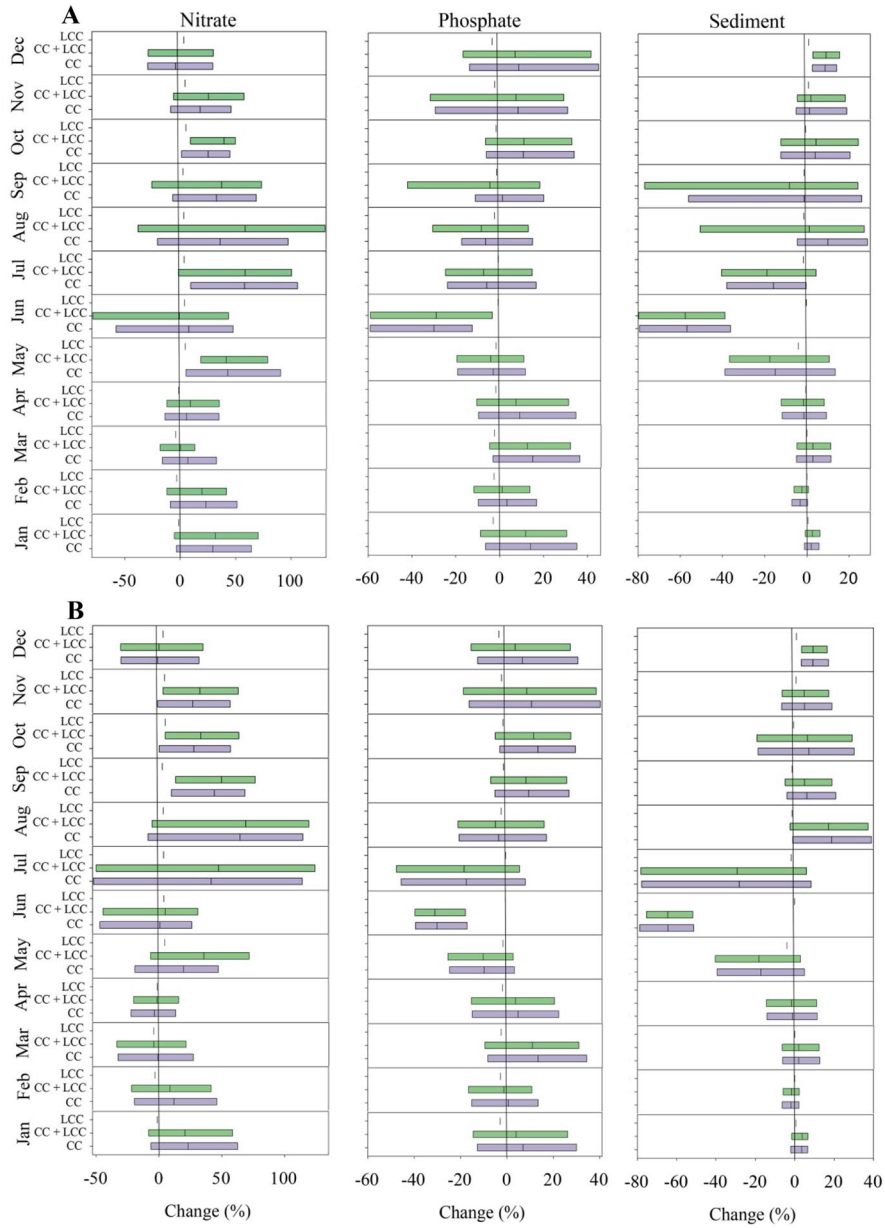

Fig. 8 Monthly changes (%) (percentile 10, average, and percentile 90 of various CMIP5 models' deltas) in nitrate, phosphate, and sediment concentrations under CC (climate change), LCC (land cover change), and CC + LCC (climate change + land cover change) for RCP 4.5 (**A**) and RCP 8.5 (**B**) scenarios. Lines indicate the position of no change

scenarios, the annual concentration of NO_3^- was found to increase by 17.3% and 15.3%, respectively, based on the inter-model average. The largest increase is forecast to occur in July by 58.2% (RCP 4.5) and in August by 64.4% (RCP 8.5) (Fig. 8). The change in annual simulated concentration of NO_3^- ranged from − 13.5% (from 0.084 to 0.073 mg N l^{-1}) (10th percentiles) to + 49.6% (from 0.084 to 0.127 mg N l^{-1}) (90th percentiles) for the RCP 4.5 scenario and from − 16.9% (10th percentiles) to + 46.3% (90th percentiles) for the RCP 8.5 scenario, based on the averages of the multi-model. Seasonal variation in the projected concentration of NO_3^- was found to increase in all seasons, with the highest increase in autumn under RCP 4.5 (22.4%; from 0.1 to 0.124 mg N l^{-1}) and RCP 8.5 (30%; from 0.1 to 0.132 mg N l^{-1}). Monthly average NO_3^- concentration increased for all months except December (−4.3%; from 0.16 to 0.153 mg N l^{-1}) under RCP 4.5 and increased for

all months except March (−1%), April (−3.8%), and December (−1.1%) under RCP 8.5 (Fig. 8). Nitrate concentration showed a maximum value in November in baseline condition (0.17 mg N l^{-1}), RCP 4.5 (0.21 mg N l^{-1}), and RCP 8.5 (0.22 mg N l^{-1}) scenarios with 2010 land cover.

The annual changes of PO_4^{3-} load for the 10th and 90th percentiles are −37.5% and + 17.6%, and −36.1% and + 27.1%, for the RCP 4.5 and RCP 8.5 scenarios, respectively, showing decreases in annual PO_4^{3-} of 9.2% and 6.2%; the largest increase would occur in January for RCP 4.5 (4.1%) and RCP 8.5 (16.8%) (Fig. 6). The seasonal concentration of PO_4^{3-} predicted by SWAT would increase by 4.8% in spring (from 5.02 to 5.27 µg P l^{-1}), 6.7% in autumn (from 6.6 to 7.03 µg P l^{-1}), and 8.7% in winter (from 3.78 to 4.1 µg P l^{-1}), decreasing by 16% in summer (from 7.34 to 6.17 µg P l^{-1}) under RCP 4.5 and increasing in autumn (11.1%) and winter (5.1%), and decreasing in spring (0.03%) and summer (17.9%) under RCP 8.5, based on the average of the multi-model. For both climate change scenarios, PO_4^{3-} concentrations decreased from May to August (Fig. 8) based on the ensemble average, with the greatest reduction in June from 9.04 µg P l^{-1} to 6.33 µg P l^{-1} under RCP 4.5 and from 9.04 µg P l^{-1} to 6.32 µg P l^{-1} under RCP 8.5. PO_4^{3-} concentrations had the largest increase in March of + 15% (from 3.33 to 3.83 µg P l^{-1}) for RCP 4.5 and + 13.4% (3.33 to 3.77 µg P l^{-1}) for the RCP 8.5. For the 10th percentile of various GCM outputs under RCP 4.5 (RCP 8.5) with 2010 land cover, a 20.6% (19.6%) reduction from 5.68 µg P l^{-1} to 4.51 (4.57) µg P l^{-1} in annual phosphate concentration was obtained, while there was an increment to 20.6% (17.4%) from 5.68 µg P l^{-1} to 6.85 (6.67) µg P l^{-1} for the 90th percentile deltas (Fig. 8). The results of nutrient modeling under CC highlight the high degree of uncertainty among various climate models.

Under the LCC scenario alone, an increase of 3.2% and 2.1%, respectively, in annual NO_3^- and PO_4^{3-} loads was observed, while an increase of 1.3% and a reduction of 1.9%, respectively, was revealed in both nutrient concentrations. Summer (+3.7%) and autumn (+4.2%) seasons showed an increase in change of nitrate concentration due to change in land cover alone and spring (−1%) and winter (−0.05%) recorded a decrease for this nutrient. All seasons exhibited a decrease in the concentration of phosphate, showing the largest decrease in winter by −3.1%. Under a reduction in annual nutrient loads based on the mean of multi-CMIP5 models, while LCC led to an annual increment in pollutants (Table 5). However, the results obtained from 10 and 90th percentile of GCM's simulations based on the multi-model revealed a marked variability of change in the nutrient loads. The RCP 4.5 scenario resulted in a 25.1% increase from 727.8 kg N to 910.5 kg N for NO_3^- loads in the 90th percentiles for various CMIP5 models, and a 26.5% reduction from 727.8 to 534.6 kg N in the 10th percentiles for the multi-model.

Combined effects of climate and land cover changes on nutrients

The largest decrease for phosphate load is projected to occur in June (32.7%; from 19.2 to 12.95 kg P) and the largest increase in December (5.4%; from 27.7 to 29.2 kg P) for RCP 4.5 combined with LCC scenario, with an annual reduction of 8.8% (Fig. 7). The annual nitrate load increased by 0.6%, with the largest increase in August (25.7%) for RCP 4.5. Under RCP 4.5, the results indicated 19.7% increase in annual nitrate concentration, and 2.2% decreases in the concentration of phosphate, based on the inter-model average. Monthly nitrate concentration was found to increase for all (ranged from + 0.21% in March to + 58.77% in August) except for the June and December under RCP 4.5 and to increase for all (ranged from + 0.05% in December to + 69.2% in August) except for the March and April under RCP 8.5 (Fig. 8). The highest seasonality average change in NO_3^- concentration was seen in autumn under both climate scenarios for which similar results were found for isolated CC scenarios. In summer, the simulated PO_4^{3-} concentration was lower under RCP 4.5 (from 7.34 to 6.12 µg P l^{-1}) than in the baseline condition, while other seasons showed increases for this nutrient (ranged from + 3.2% to + 6.8%).

Simulation of combined changes resulted in a 3% increase in NO_3^- load, and a 4.3% decrease in PO_4^{3-} load under RCP 8.5 (Table 5). The 10th percentiles for annual NO_3^- and PO_4^{3-} load showed a reduction of 26.3% and 34.5%, respectively, and increases of 31.5% and 29.4% for the two contaminants for the 90th percentiles under RCP 8.5. The analyses of combined LCC and CC (RCP 8.5 scenario) showed that the annual change of the NO_3^- and PO_4^{3-} concentrations were + 17.8% and −3.2%, respectively, based

on the mean of various CMIP5 models. The effects of LCC and RCP 8.5 scenario estimates were a 1.2% decrease of phosphate concentration in spring and a 19% decrease in summer, while they increased by 2.4% in winter and 9.4% in autumn.

Table 5 shows the mean annual simulated variation (scenarios vs. baseline) of water quantity and quality parameters based on the inter-model average. The average annual nitrate load showed a slight change in all scenarios, while showing marked variability in the 10th and 90th percentiles for the multi-model of GCM. Average simulated NO_3^- load was 957 (536) kg N for the 90th (10th) percentile of various GCM outputs under combination of LCC, and RCP 8.5, relative to the historical annual average of 727.8 kg N in the baseline condition. For the joint change in land cover and RCPv8.5, phosphate load ranged from 18.4 to 36.3 kg P for the 10th and 90th percentiles.

Discussion

In this study, we ran the SWAT model for simulating water quality under future climate change induced in land cover, which was previously calibrated for discharge to assess the potential effects on the water balance components of the Neka River basin. The increase in agricultural, rangeland, and residential areas and the decrease in forest area projected for the land cover in 2050 with the observed climate data indicates that the annual sediment yield, nitrate, and phosphate loads in the Neka River basin will increase compared with those under the 2010 land cover conditions. LCC appears to have minimal effect on surface water quality relative to CC and pollutant loads for the land cover of 2050, which were higher than those for the land cover of 2010. This suggests that the agricultural intensification (mainly conversion of forest to agriculture) and excessive fertilization are the main sources of soil erosion and incremental nutrient loads in the Neka River basin. However, the relative reduction in the land areas affected by LCC (Joorabian Shooshtari et al., 2018) may explain the relatively less impact of LCC on both the sediment and nutrients loads. Since the changes in water quality parameters under LCC were small, CC scenarios are the main controlling factor of change in the future loads of nutrients in the Neka River basin. This may be due to the fact that sediment carries a large portion of the contaminants which is highly sensitive to precipitation and discharge and its relationship with the discharge is usually as a power function (Azari et al., 2016). Under CC, increased precipitation especially extreme rainfall can lead to an increase in sediment yield as well as water contaminants (Abbaspour et al., 2009). Thus, the effects of climate changes on water quality chemistry are greater than those of LCCs. The annual predicted discharge in land cover for the year 2050 was higher than that simulated under land cover observed in 2010 in the Neka River basin (Joorabian Shooshtari et al., 2017). This might be related to the decrease in the evapotranspiration, and infiltration rates, and an increase in surface runoff and river discharge volume as consequences of the degradation of natural ecosystems, residential development, and agricultural expansion. Therefore, increased discharge under LCC led to a small increase in average annual sediment yield. Conversion from forest to agricultural land led to an increased amount and velocity of surface runoff and, as a result, an increase in sediment loadings (García-Ruiz et al., 2010). Phosphate mostly moves attached to sediment; consequently, the average annual PO_4^{3-} yield increased in the watershed. Simulated PO_4^{3-} yield by SWAT is expected to follow a pattern similar to sediment yield. The increase of nitrate and phosphate as a reaction of the basin is correlated with agricultural expansion, residential development, and deforestation. Nutrients can be lost from deforested areas by increased mobilization of soil nutrients and leaching, especially when little vegetation is available to take up nutrients (Hajabbasi et al., 1997). Some essential sources of nutrients in the river include fertilizers used in agricultural activities, detergents from residential sewage due to population growth. Future LCC scenarios exhibit a higher impact on nitrate loads than the sediment and phosphate loads in the Neka River basin. This is probably due more to greater urea fertilizers' consumption with high leaching in intensive agricultural areas than to phosphorus fertilizer locations in which the urea manure is out of reach of the roots, leading to leaching into groundwater and an increased in the load of nitrate on the surface waters.

The average annual sediment is expected to change from 207.1 to 190.2 tons for the RCP 4.5 scenario and based on the ensemble mean. We have projected annual decreases in sediment yield of 8.1% for RCP 4.5 and 1.6% for RCP 8.5 scenarios, mostly due to

the decline in predicted annual river discharge for this basin (see Joorabian Shooshtari et al., 2017). A strong relationship between discharge and sediment (R^2: 0.98 under baseline condition) was evident in the Neka River basin. Predicted precipitation is the main factor affecting the reduction in simulated river discharge (Joorabian Shooshtari et al., 2017), which in turn is also the main driver of reduced sediment load in the Neka River basin. These results are in agreement with the findings of previous studies. Perazzoli et al. (2012) used SWAT to assess the hydrological response under climate changes in southern Brazil and reported that sediment yield follows the same pattern as discharge. The same results were reported by Serpa et al. (2015) in the São Lourenço catchment, Spain, reporting that the decreases in simulated annual precipitation would lead to a decrease in the annual discharge and sediment export. Under the CC-only scenarios, reduction in NO_3^- was linked with a decreased magnitude of the discharge in the present study, except that some months showed different behaviors. Nitrate correlation with discharge is 0.70 under the baseline conditions. These results agree with the findings of Molina-Navarro et al. (2014) in the Ompólveda River basin, Spain. Varanou et al. (2002) also reported that decreasing surface and lateral flows diminished nitrate losses in the Ali Efenti Basin, central Greece. Our analysis illustrated that the highest increase in temperature is projected for summer under the two RCPs, and the large decrease in nitrate estimates occurs in the summer months because of the increase in temperature, which could also lead to more losses of nitrate due to the increase of mineralization (Molina-Navarro et al., 2018).

The annual PO_4^{3-} load of the basin is expected to decrease under both CC scenarios. Generally, similar trends of discharge variation were observed for the PO_4^{3-} load. Additionally, a positive correlation was found between sediment yield and phosphate load ($R^2 = 0.85$), which indicated that PO_4^{3-} transport is mostly controlled by sediment in the catchment and this nutrient mainly came from soil erosion and fertilizer input from the area covered by cultivated land. The differences in the annual pollutant loss reductions can be attributed to different transport pathways of these compounds into surface waters. Despite the decrease in annual loads of water quality parameters, the concentration of nitrate in the two RCPs showed a significant increase based on the ensemble mean, which is due to the reduction of the water dilution rate with a decrease in river discharge (Serpa et al., 2017). The amount of sediment yield showed less change (from 207.1 to 194.0 tons) in joint CC and LCC as compared to the existing scenario (Table 5). The change in the average annual load of nitrate is simulated to decrease only from 727.8 to 713.9 kg N under RCP 4.5 alone (a change of around 14 kg N), but increased only from 727.8 to 732 kg N (change of 4 kg N) for the combined CC and LCC simulations. Changes in the response of annual water quality parameters to impacts of CC and LCC are less than that of CC alone, especially for the RCP 4.5 scenario, reflecting LCC highlights of the role of compensation in the annual loads under future CC relative to the baseline climate.

Figure 6 depicts the monthly sediment yield, nitrate, and phosphate load estimations that tend to be quite variable under CC scenarios. The inter-model variability for future precipitation and R10mm index is very big, and this is a constraint to project properly the magnitude of monthly runoff and flood events that tightly control sediment and nutrient loads. There are several sources of uncertainty in the water quality models, including model structural uncertainty and state uncertainty, input data uncertainty (changes in the natural conditions, limitations in instrument such as detection limit, and insufficient and short length of observed data), and parameter uncertainty (Shen et al., 2010). The sources of uncertainty in hydrological modeling stem from applying future CC projections that are mostly linked to climate change scenario uncertainty, structural uncertainty of GCM, GCM initial conditions (ensemble runs), and a choice of downscaling methods from GCMs (Prudhomme and Davies, 2009; Chen et al., 2011b; Mehdi et al., 2015). In the current study, to increase the range of future projections, an ensemble of 17 future GCM simulations was run to investigate hydrological effects on a watershed that led to a different range with high variability of outcomes. As suggested by some researches, an effective way to obtain the variability change in water quality under CC conditions and improve results of the model, it is more robust to analyze several GCMs (Shrestha et al., 2017) and downscaling methods (Chen et al., 2011a), instead of focusing on a single model, in order to interpret results with more caution and to cover a wider range of variability. Another source of uncertainty in this research is using a delta change factor because the temporal length of wet or dry days and variances of temperatures are not taken into account, which influences the reliability of our

results (Chen et al., 2011a). One of the main inputs for hydrological modeling in SWAT is soil characteristics. The main limitation in input data is related to the lack of high-resolution soil map and daily measured nutrient data in the Neka River basin; therefore we used a low-resolution FAO's global soil map as input to the hydrological model. This global map was applied in watersheds where the local map was unavailable at a finer scale. Accessibility to the detailed soil data was the main limitation of this research, which should be addressed in follow-up studies. Bouslihim et al. (2019) concluded that an insignificant variation has been observed in stream flow simulation between a refined database with eleven soil classes and FAO soil map, but these two soil databases mainly affected the SWAT model predictions of soil water content and water yield in Tamedroust watershed, Morocco. The findings of the Chaplot (2005) concluded that the more time, effort, and extra cost to produce more detailed soil data with the highest accuracy is not justified to obtain more accurate simulation in the Lower Walnut Creek. Given the precautions taken from those results, when applied to other models or case studies, only a limited amount of water quality data (1 or 2 days of data per month) was available in the study zone; consequently, LOADEST (LOAD ESTimator) software, developed by USGS, was utilized to reconstruct time series of nutrient data and to fill in missing data. LOADEST has been previously applied to estimate daily values of nutrient loads over a time period in several studies, such as that of Yen et al. (2015) and Niraula et al. (2013). Another limitation to this study's approach was the uncertainty of the observed data, due to scarcity in the water quality observation data and estimated by LOADEST, which impact model output integrity (Hoque et al., 2012). Land cover impact assessments on hydrological modeling are plagued with several source uncertainties, such as decision makers' behavior in the future, which may change the position of new settlements and agricultural development in the future, according to changes in national and regional policy. These limitations may have had an impact on modeling, but this was inevitable.

Conclusions

SWAT model, a quasi-distributed hydrological model, was used to evaluate the effects of future LCC and CC on the surface water quality in the Neka River basin, Iran. Reasonable agreement between observed and projected data of sediment, phosphate, and nitrate loads suggests that the SWAT model can be recognized as a valuable tool for the impact analysis of water quality parameters under combined CC and LCC. Future climate emission scenarios showed a trend of warmer climate conditions with large inter-model variability in the basin's precipitation for the period 2035−2065. Climate and land cover change impact analyses revealed that both annual sediment and phosphate concentrations are likely to decrease and nitrate concentration to increase in the future under the inter-model average. An increase is observed in the sediment, phosphate, and nitrate for all of the months under LCC, because of the expansion of cultivated lands, increased erosion rate, and higher fertilizer application. Our analysis indicated that the impacts of LCC would be less than those caused by the projected CC. Simulations of water quality parameters are subject to high uncertainties under CC due to the model's large uncertainties in the predicting of precipitation. Change in rainfall has a pronounced impact on pollutants because of the change in discharge and sediment yield. Several sources of uncertainty suggest that model results should be interpreted with great care. However, this study may be beneficial to land managers of the Neka River basin, as it clearly illustrates how water quality can deteriorate in response to changes in CC and LCC.

Acknowledgements We sincerely thank the Pyrenean Institute of Ecology and the Spanish National Research Council (CSIC) for welcoming the first author as a visiting researcher during his Ph.D. studies. The authors thank Javier Zabalza (IPE) and Eugenio Molina-Navarro (Aarhus University) for their guidance and valuable comments.

Funding This research was financially supported by Malayer University, Iran, under grant number 84/5–205. The authors are grateful for the sponsorship of the Ministry of Science, Research, and Technology of Iran and the National Elites Foundation during the sabbatical of S. Joorabian Sooshtari.

Data availability Data will be made available on reasonable request.

References

Abbaspour, K.C. (2015). SWAT-CUP 2012/Calibration and Uncertainty Programs.

Abbaspour, K. C., Yang, J., Maximov, I., Siber, R., Bogner, K., Mieleitner, J., Zobrist, J., & Srinivasan, R. (2007). Modelling hydrology and water quality in the pre-alpine/alpine Thur watershed using SWAT. *Journal of Hydrology., 333*(2–4), 413–430. https://doi.org/10.1016/j.jhydrol.2006.09.014

Abbaspour, K. C., Faramarzi, M., Ghasemi, S. S., & Yang, H. (2009). Assessing the impact of climate change on water resources in Iran. *Water Resource Research, 45*(10), 1–16. https://doi.org/10.1029/2008WR007615

Aboelnour, M., Gitau, M. W., & Engel, B. A. (2020). A comparison of streamflow and baseflow responses to land-use change and the variation in climate parameters using SWAT. *Water, 12*, 191. https://doi.org/10.3390/w12010191

Anand, J., Gosain, A. K., & Khosa, R. (2018). Prediction of land use changes based on Land Change Modeler and attribution of changes in the water balance of Ganga basin to land use change using the SWAT model. *Science of the Total Environment, 644*, 503–519. https://doi.org/10.1016/j.scitotenv.2018.07.017

Ashraf Vaghefi, S., Mousavi, S. J., Abbaspour, K., Srinivasan, R., & Yang, H. (2014). Analyses of the impact of climate change on water resources components, drought and wheat yield in the semi-arid Karkheh River Basin in Iran. *Hydrological Processes, 28*(4), 2018–2032. https://doi.org/10.1002/hyp.9747

Azari, M., Moradi, H. R., Saghafian, B., & Faramarzi, M. (2016). Climate change impacts on streamflow and sediment yield in the North of Iran. *Hydrological Sciences Journal, 61*(1), 123–133. https://doi.org/10.1080/02626667.2014.967695

Baker, T. J., & Miller, S. N. (2013). Using the Soil and Water Assessment Tool (SWAT) to assess land use impact on water resources in an East African watershed. *Journal of Hydrology, 486*, 100–111. https://doi.org/10.1016/j.jhydrol.2013.01.041

Boix-Fayos, C., Vente, J., Martínez-Mena, M., Barberá, G. G., & Castillo, V. (2008). The impact of land use change and check-dams on catchment sediment yield. *Hydrological Processes, 22*, 4922–4935. https://doi.org/10.1002/hyp.7115

Bouslihim, Y., Rochdi, A., Amrani Paaza, N. E., & Liuzzo, L. (2019). Understanding the effects of soil data quality on SWAT model performance and hydrological processes in Tamedroust watershed (Morocco). *Journal of African Earth Sciences, 160*, 103616. https://doi.org/10.1016/j.jafrearsci.2019.103616

Chaplot, V. (2005). Impact of DEM mesh size and soil map scale on SWAT runoff, sediment, and NO3–N loads predictions. *Journal of Hydrology, 312*, 207–222. https://doi.org/10.1016/j.jhydrol.2005.02.017

Chen, J., Brissette, F. P., & Leconte, R. (2011a). Uncertainty of downscaling method in quantifying the impact of climate change on hydrology. *Journal of Hydrology, 401*(3–4), 190–202. https://doi.org/10.1016/j.jhydrol.2011.02.020

Chen, J., Brissette, F. P., Poulin, A., Leconte, R. (2011b). Overall uncertainty study of the hydrological impacts of climate change for a Canadian watershed. *Water Resources Research, 47*(12). https://doi.org/10.1029/2011WR010602

Choubin, B., Solaimani, K., Rezanezhad, F., Habibnejad Roshan, M., Malekian, A., & Shamshirband, S. (2019). Streamflow regionalization using a similarity approach in ungauged basins: Application of the geo-environmental signatures in the Karkheh River Basin. *Iran. Catena, 182*, 104128. https://doi.org/10.1016/j.catena.2019.104128

Deng, Z., Zhang, X., Li, D., & Pan, G. (2015). Simulation of land use/land cover change and its effects on the hydrological characteristics of the upper reaches of the Hanjiang Basin. *Environment and Earth Science, 73*, 1119–1132. https://doi.org/10.1007/s12665-014-3465-5

Eastman, J. R., Van Fossen, M. E., & Solorzano, L.A. (2005). Transition potential modeling for land cover change. In: D. J. Maguire, D. J. Batty, M. F. Goodchild (Eds.), *GIS, Spatial Analysis and Modeling* (357–386). ESRI Press, Redlands, CA.

El-Khoury, A., Seidou, O., Lapen, D. R., Que, Z., Mohammadian, M., Sunohara, M., & Bahram, D. (2015). Combined impacts of future climate and land use changes on discharge, nitrogen and phosphorus loads for a Canadian river basin. *Journal of Environmental Management, 151*, 76–86. https://doi.org/10.1016/j.jenvman.2014.12.012

Fan, M., & Shibata, H. (2015). Simulation of watershed hydrology and stream water quality under land use and climate change scenarios in Teshio River watershed, northern Japan. *Ecological Indicators, 50*, 79–89. https://doi.org/10.1016/j.ecolind.2014.11.003

Ficklin, D. L., Luo, Y., & Zhang, M. (2013). Watershed modelling of hydrology and water quality in the Sacramento River watershed, California. *Hydrological Processes, 27*, 236–250. https://doi.org/10.1002/hyp.9222

Fowler, H. J., Blenkinsop, S., & Tebaldi, C. (2007). Linking climate change modelling to impacts studies: Recent advances in downscaling techniques for hydrological modeling. *International Journal of Climatology, 27*, 1547–1578. https://doi.org/10.1002/joc.1556

García-Ruiz, J. M., Lana-Renault, N., Beguería, S., Lasanta, T., Regués, D., Nadal-Romero, E., Serrano-Muela, P., López-Moreno, J. I., Alvera, B., Martí-Bono, C., & Alatorre, L. C. (2010). From plot to regional scales: Interactions of slope and catchment hydrological and geomorphic processes in the Spanish Pyrenees. *Geomorphology, 120*, 248–257. https://doi.org/10.1016/j.geomorph.2010.03.038

Ghanbarpour, M. R., Mohseni Saravi, H., & Salimi, S. (2014). Floodplain inundation analysis combined with contingent valuation: Implications for sustainable flood risk management. *Water Resources Management, 28*(9), 2491–2505. https://doi.org/10.1007/s11269-014-0622-2

Glavan, M., Ceglar, A., & Pintar, M. (2015). Assessing the impacts of climate change on water quantity and quality modelling in small Slovenian Mediterranean catchment—lesson for policy and decision makers. *Hydrological Processes, 29*(14), 3124–3144. https://doi.org/10.1002/hyp.10429

Hajabbasi, M. A., Jalalian, A., & Karimzadeh, H. R. (1997). Deforestation effects on soil physical and chemical properties, Lordegan. *Iran. Plant Soil, 190*, 301–308. https://doi.org/10.1023/A:1004243702208

Hoque, Y. M., Tripathi, S., Hantush, M. M., & Govindaraju, R. S. (2012). Watershed reliability, resilience and vulnerability analysis under uncertainty using water quality data. *Journal of Environmental Management, 109*, 101–112. https://doi.org/10.1016/j.jenvman.2012.05.010

Hosseini, M., Ghafouri, M. A., Amin, M. S. M., Tabatabaei, M. R., Goodarzi, M., & Abde Kolahchi, A. (2012). Effects of land use changes on water balance in Taleghan catchment.

Iran. Journal of Agricultural Science and Technology, 14(5), 1159–1172.

IPCC. (2013). Climate change 2013: the physical science basis, IPCC Contribution of Working Group I to the Fifth Assessment Report of the Intergovernmental Panel on Climate Change. Cambridge University Press, Cambridge.

Joorabian Shooshtari, S., & Gholamalifard, M. (2015). Scenario-based land cover change modeling and its implications for landscape pattern analysis in the Neka Watershed. *Iran. Remote Sensing Applications: Society and Environment, 1*, 1–19. https://doi.org/10.1016/j.rsase.2015.05.001

Joorabian Shooshtari, S., Hosseini, S. M., Esmaili-Sari, A., & Gholamalifard, M. (2012). Monitoring land cover change, degradation, and restoration of the Hyrcanian forests in northern Iran (1977–2010). *International Journal of Environmental Sciences, 3*(3), 1038–10563. https://doi.org/10.6088/ijes.2012030133012

Joorabian Shooshtari, S., Shayesteh, K., Gholamalifard, M., Azari, M., López-Moreno, J. I. (2018). Land cover change modelling in Hyrcanian forests, northern Iran: a landscape pattern and transformation analysis perspective. *Cuadernos de Investigación Geográfica, 44*(2):743–761. https://doi.org/10.18172/cig.3279

Joorabian Shooshtari, S., Shayesteh, K., Gholamalifard, M., Azari, M., Serrano-Notivoli, R., & López-Moreno, J. I. (2017). Impacts of future land cover and climate change on the water balance in northern Iran. *Hydrological Sciences Journal, 62*(16), 2655–2673. https://doi.org/10.1080/02626667.2017.1403028

Kibii, J. K., Kipkorir, E. C., & Kosgei, J. R. (2021). Application of Soil and Water Assessment Tool (SWAT) to evaluate the impact of land use and climate variability on the Kaptagat catchment river discharge. *Sustainability, 13*, 1802. https://doi.org/10.3390/su13041802

Lenhart, T., Fohrer, N., & Frede, H. (2003). Effects of land use changes on the nutrient balance in mesoscale catchments. *Physics and Chemistry of the Earth, 28*, 1301–1309. https://doi.org/10.1016/j.pce.2003.09.006

Lin, Y. P., Hong, N. M., Wu, P. J., & Lin, C. J. (2007). Modeling and assessing land-use and hydrological processes to future land-use and climate change scenario in watershed land-use planning. *Environmental Geology, 53*, 623–634. https://doi.org/10.1007/s00254-007-0677-y

Mas, J. F., Kolb, M., Paegelow, M., Carmacho Olmedo, M. T., Houet, T. (2014). Inductive pattern-based land use/cover change models: a comparison of four software packages. *Environmental Modeling & Software, 51*:94–111. https://doi.org/10.1016/j.envsoft.2013.09.010

Mehdi, B., Ludwig, R., & Lehner, B. (2015). Evaluating the impacts of climate change and crop land use change on streamflow, nitrates and phosphorus: A modeling study in Bavaria. *Journal of Hydrology Regional Studies, 4*, 60–90. https://doi.org/10.1016/j.ejrh.2015.04.009

Moghadam, N. T., Abbaspour, K. C., Malekmohammadi, B., Schirmer, M., & Yavari, A. R. (2021). Spatiotemporal modelling of water balance components in response to climate and land use changes in a heterogeneous mountainous catchment. *Water Resources Management, 35*, 793–810. https://doi.org/10.1007/s11269-020-02735-w

Molina-Navarro, E., Andersen, H. E., Nielsen, A., Thodsen, H., & Trolle, D. (2018). Quantifying the combined effects of land use and climate changes on stream flow and nutrient loads: A modelling approach in the Odense Fjord catchment (Denmark). *Science of the Total Environment, 621*, 253–264. https://doi.org/10.1016/j.scitotenv.2017.11.251

Molina-Navarro, E., Trolle, D., Martinez-Perez, S., Sastre-Merlin, A., & Jeppesen, E. (2014). Hydrological and water quality impact assessment of a Mediterranean limno-reservoir under climate change and land use management scenarios. *Journal of Hydrology, 509*, 354–366. https://doi.org/10.1016/j.jhydrol.2013.11.053

Neitsch, S. L., Arnold, J. G., Kiniry, J. R., Williams, J. R. (2011). Soil and Water Assessment Tool Theoretical Documentation version 2009, 2011. Texas Water Resources Institute Technical Report No. 406. Texas A&M University System, Texas.

Nguyen, H. H., Recknagel, F., Meyer, W., Frizenschaf, J., Ying, H., & Gibbs, M. S. (2019). Comparison of the alternative models SOURCE and SWAT for predicting catchment streamflow, sediment and nutrient loads under the effect of land use changes. *Science of the Total Environment, 662*, 254–265. https://doi.org/10.1016/j.scitotenv.2019.01.286

Niraula, R., Kalin, L., Srivastava, P., & Anderson, C. J. (2013). Identifying critical source areas of nonpoint source pollution with SWAT and GWLF. *Ecological Modelling, 268*, 123–133. https://doi.org/10.1016/j.ecolmodel.2013.08.007

Perazzoli, M., Pinheiro, A., & Kaufmann, V. (2012). Assessing the impact of climate change scenarios on water resources in southern Brazil. *Hydrological Sciences Journal, 58*(1), 77–87. https://doi.org/10.1080/02626667.2012.742195

Pirnia, A., Darabi, H., Choubin, B., Omidvar, E., Onyutha, C., & Haghighi, A. T. (2019). Contribution of climatic variability and human activities to stream flow changes in the Haraz River basin, northern Iran. *Journal of Hydro-Environment Research, 25*, 12–24. https://doi.org/10.1016/j.jher.2019.05.001

Prudhomme, C., & Davies, H. (2009). Assessing uncertainties in climate change impact analyses on the river flow regimes in the UK. Part 2: Future climate. *Climate Change, 93*, 197–222. https://doi.org/10.1007/s10584-008-9461-6

Rajaei, F., Esmaili Sari, A., Salmanmahiny, A., Delavar, M., Massah Bavani, A. R., & Srinivasan, R. (2017). Surface drainage nitrate loading estimate from agriculture fields and its relationship with landscape metrics in Tajan watershed. *Paddy and Water Environment, 15*, 541–552. https://doi.org/10.1007/s10333-016-0570-y

Runkel, R. L., Crawford, C. G., Cohn, T. A. (2004). Load estimator (Loadest): a Fortran program for estimating constituent loads in streams and rivers. USGS Science For A Changing World, Techniques and Methods Book 4, Chapter A5.

Sangermano, F., Toledano, J., & Eastman, J. R. (2012). Land cover change in the Bolivian Amazon and its implications for REDD+ and endemic biodiversity. *Landscape Ecology, 27*, 571–584. https://doi.org/10.1007/s10980-012-9710-y

Serpa, D., Nunes, J. P., Keizer, J. J., Abrantes, N. (2017). Impacts of climate and land use changes on the water quality of a small Mediterranean catchment with intensive viticulture. *Environmental Pollution,* 1–12. https://doi.org/10.1016/j.envpol.2017.02.026

Serpa, D., Nunes, J. P., Santos, J., Sampaio, E., Jacinto, R., Veiga, S., Lima, J. C., Moreira, M., Corte-Real, J., Keizer, J. J., & Abrantes, N. (2015). Impacts of climate and land use changes on the hydrological and erosion processes of two contrasting Mediterranean catchments. *Science of the Total Environment, 538*, 64–77. https://doi.org/10.1016/j.scitotenv.2015.08.033

Shen, Z., Hong, Q., Yu, H., & Niu, J. (2010). Parameter uncertainty analysis of non-point source pollution from different land use types. *Science of the Total Environment, 408*, 1971–1978. https://doi.org/10.1016/j.scitotenv.2009.12.007

Shrestha, M. K., Recknagel, F., Frizenschaf, J., & Meyer, W. (2017). Future climate and land uses effects on flow and nutrient loads of a Mediterranean catchment in South Australia. *Science of the Total Environment, 590–591*, 186–193. https://doi.org/10.1016/j.scitotenv.2017.02.197

Tamm, O., Maasikamäe, S., Padari, A., & Tamm, T. (2018). Modelling the effects of land use and climate change on the water resources in the eastern Baltic Sea region using the SWAT model. *CATENA, 167*, 78–89. https://doi.org/10.1016/j.catena.2018.04.029

Varanou, E., Gkouvatsou, E., Baltas, E., & Mimikou, M. (2002). Quantity and quality integrated catchment modeling under climate change with use of Soil and Water Assessment Tool Model. *Journal of Hydrologic Engineering, 7*, 228–244.

Verma, S., Bhattarai, R., Bosch, N. S., Cooke, R. C., Kalita, P. K., & Markus, M. (2015). Climate change impacts on flow, sediment and nutrient export in a great lakes watershed using SWAT. *CLEAN - Soil Air Water, 43*(11), 1464–1474. https://doi.org/10.1002/clen.201400724

Vicente-Serrano, S. M., López-Moreno, J. I., Beguería, S., Lorenzo-Lacruz, J., Sanchez-Lorenzo, A., García-Ruiz, J. M., Azorin-Molina, C., Morán-Tejeda, E., Revuelto, J., Trigo, R., Coelho, F., Espejo, F. (2014). Evidence of increasing drought severity caused by temperature rise in southern Europe. *Environmental Research Letters, 9*(044001). https://doi.org/10.1088/1748-9326/9/4/044001

Wilby, R. L., Harris, I., (2006). A framework for assessing uncertainties in climate change impacts: low-flow scenarios for the River Thames, UK. *Water Resources Research, 42*(2). https://doi.org/10.1029/2005WR004065

Williams, J. R., & Berndt, H. D. (1977). Sediment yield prediction based on watershed hydrology. *Transactions of ASAE, 20*(6), 1100–1104. https://doi.org/10.13031/2013.35710

Wu, H., & Chen, B. (2015). Evaluating uncertainty estimates in distributed hydrological modeling for the Wenjing River watershed in China by GLUE, SUFI-2, and ParaSol methods. *Ecological Engineering, 76*, 110–121. https://doi.org/10.1016/j.ecoleng.2014.05.014

Yen, H., Hoque, Y., Harmel, R. D., & Jeong, J. (2015). The impact of considering uncertainty in measured calibration/validation data during auto-calibration of hydrologic and water quality models. *Stochastic Environmental Research and Risk Assessment, 29*, 1891–1901. https://doi.org/10.1007/s00477-015-1047-z

Zhang, Z., Chen, S., Wan, L., Cao, J., Zhang, Q., & Yang, C. (2021). The effects of landscape pattern evolution on runoff and sediment based on SWAT model. *Environmental Earth Sciences, 80*, 2. https://doi.org/10.1007/s12665-020-09315-6